Structure, Acidity, and Redox Aspects of VOx/ZrO$_2$/SiO$_2$ Catalysts for the n-Butane Oxidative Dehydrogenation

José-Luis Sánchez-García [1] , **Brent E. Handy [1]**, **Ilse N. Ávila-Hernández [1]**,
Angel G. Rodríguez [2] , **Ricardo García-Alamilla [3] and Maria-Guadalupe Cardenas-Galindo [1],***

[1] Facultad de Ciencias Químicas, Universidad Autónoma de San Luis Potosí (UASLP), Av. Manuel Nava #6, San Luis Potosí, S.L.P. 78210, Mexico; luis.sanchez@uaslp.mx (J.-L.S.-G.); handy@uaslp.mx (B.E.H.); ilse3571@hotmail.com (I.N.Á.-H.)

[2] Coordinación para la Innovación y la Aplicación de la Ciencia y la Tecnología, UASLP, Álvaro Obregón 64, San Luis Potosí, S.L.P. 78000, Mexico; angel.rodriguez@uaslp.mx

[3] Centro de Investigación en Petroquímica, Tecnológico Nacional de México, Instituto Tecnológico de Ciudad Madero, Altamira, Tamps 89600, Mexico; ricardogarcia.alamilla@yahoo.com.mx

* Correspondence: cardenas@uaslp.mx; Tel.: +52-444-826-2440 (ext. 6468)

Abstract: ZrOx/SiO$_2$ and VOx/ZrO$_x$/SiO$_2$ catalysts (5 wt %–25 wt % Zr, 4 wt % V) were prepared by grafting zirconium and vanadium alkoxides on Aerosil 380. All samples were characterized by temperature programmed reduction, N$_2$ physisorption, X-ray diffraction, Raman spectroscopy, and ammonia adsorption microcalorimetry. Tetragonal ZrO$_2$ and zircon (ZrSiO$_4$) were present at 25 wt % Zr, but only amorphous zirconia overlayer existed for lower loadings. At lower Zr loadings (5 wt %–10 wt % Zr), exposed silica surface leads to V$_2$O$_5$ crystallites and isolated VO$_4$ species, although V reducibility behavior changes, from being similar to VOx/SiO$_2$ (5 wt % Zr) to showing VOx/ZrO$_2$ behavior at 10 wt % Zr, and a diminished total amount of reducible V. Highly acidic ZrO$_2$ sites are covered by the vanadium grafting, forming weaker sites (60–100 kJ/mol NH$_3$ adsorption strength). Catalytic conversion and selectivity for the oxidative dehydrogenation of n-butane (673 K, n-C$_4$/O$_2$ = 2.2) over VOx/ZrOx/SiO$_2$ show that 1,3-butadiene is favored over cis-2-butene and trans-2-butene, although there is some selectivity to the 2-butenes when VOx/ZrO$_2$ behavior is evident. At low Zr loadings, butadiene formed during reaction acts as the diene species in a Diels–Alder reaction and gives rise to a cyclic compound that undergoes further dehydrogenation to produce benzaldehyde.

Keywords: V$_2$O$_5$/ZrO$_2$; butane ODH; adsorption microcalorimetry; TPR; Raman; Diels–Alder

---

1. Introduction

The last few years have seen a growing interest in cycloaddition reactions, such as Diels–Alder, followed by dehydrogenation to produce aromatic compounds in a novel fashion from diverse feedstocks, such as those that come from biomasses [1]. An important aromatic compound used in the food, perfume, and pharmaceutical industry is benzaldehyde, with the requirement that it must be free of toxic impurities. Currently, commercial benzaldehyde production occurs by either toluene oxidation or the hydrolysis of benzal chloride. However, both processes cannot be considered as green technologies, as the benzaldehyde produced may contain benzoic acid or chlorine residues [2] that must be removed, which complicates the design of the separation process system. In the past decade, interest has been focused on the heterogeneous oxidation of benzyl alcohol to benzaldehyde [3–9],

a cleaner route to chlorine-free benzaldehyde owing to the low toxicity of benzyl alcohol, although with the disadvantage that the benzyl alcohol requires benzyl chloride hydrolysis for its production.

　　Another research area of high interest is the oxidative-dehydrogenation (ODH) of n-butane to produce butadiene. This process offers an alternative to the high energy consumption process based on n-butane dehydrogenation. The formation of both oxidation and dehydrogenation products during ODH opens the possibility for favoring selectivity towards one of these products if the catalyst is tailored to the right characteristics. Butadiene, the product of interest in n-butane ODH, is a diene that, in the presence of a dienophile, can react via a Diels–Alder mechanism to form a cycloaddition product. For instance, butadiene and acrolein (2-propenal) form 3-cyclohexene-1-carboxaldehyde, which, in the presence of an ODH catalyst, could undergo further dehydrogenation to produce benzaldehyde (Scheme 1).
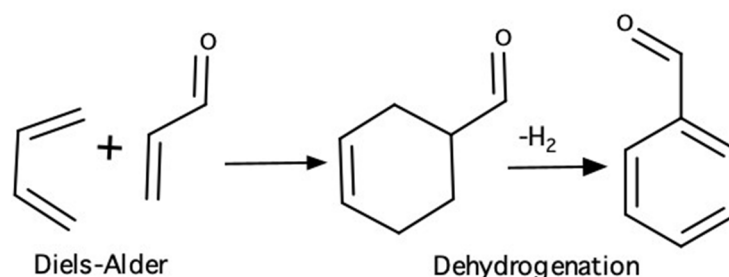
Scheme 1. Reactions involved in the formation of benzaldehyde from butadiene and acrolein.

　　This represents an alternative method for benzaldehyde production, where the use of an ODH catalyst could make the direct conversion of n-butane to benzaldehyde possible [10]. This process represents an attractive novel route to produce benzaldehyde, as the separation of the reaction products would be facilitated by the differences in the physical and chemical properties of the products (i.e., relative volatilities). Additionally, none of the components present will have a toxicity approaching that of chlorinated products, making it possible to have a greener technology than those offered by established processes or those under development.

　　A catalyst for this process should favor the formation not only of butadiene, but also of acrolein, which would successively lead to benzaldehyde. These two compounds could be formed in similar amounts given the right balance of redox and acid sites of appropriate type and strength on the catalyst.

　　An important factor in ODH of butane (to form butadiene) is the balance between acidic and basic sites. Acidity is required to promote the alkane activation; however, strong acidity will result in more oxidation products (COx), reducing the selectivity to olefins. Therefore, it is desirable to control the acidity of the catalyst. The control of acidity is also an important factor in the reduction of the cracking reactions observed in ODH of butane, attributed to highly acidic Lewis sites on the catalytic surface [11]. However, cracking products are not the only products observed in ODH of butane. Partial oxidation products (i.e., acrolein) are frequently detected in studies of this reaction over different materials [12] and the reducibility (redox sites) of the catalyst has an effect on their formation [13]. Additionally, basic sites favor the desorption of the olefins, and further oxidation can be minimized [14–16]. The catalytic materials used in oxidation and dehydrogenation of butane are very complex and it is clear that the combination of acid, basic, and redox properties determines the selectivity to dehydrogenation, partial, or complete oxidation products.

　　Vanadium-based catalysts are among the materials that have been extensively studied for alkane ODH [17]. Its acid–base and redox properties and the VOx structure on the surface depend on the type of support. SiO_2, ZrO_2, and γ-Al_2O_3 have been commonly used in n-butane ODH studies [18–21]. Zirconia possesses acidic as well as basic surface sites, and has demonstrated catalytic activity for CO oxidation [22,23], methanol oxidation [24,25], and oxidative dehydrogenation of hydrocarbons [16,26]. It also possesses ceramic properties such as high chemical resistance, thermal stability, mechanical hardness, and ionic conductivity at high temperature, but also suffers from low surface area. On the

other hand, amorphous silica can be synthesized as a high surface area and mesoporous support material, though it is not mechanically stable in the presence of water at high temperatures. Supports composed of ZrO_2/SiO_2 are of interest for catalytic applications because they offer mechanical resistance to alkaline corrosion and possess very low thermal expansion.

In propane ODH, VOx/ZrO_2 is more active than VOx/SiO_2, but the selectivity to propylene is higher with lower activity [27]. If VOx is supported on mixed ZrO_2-SiO_2, the selectivity to partial oxidation products in alcohol oxidations improves in comparison with V_2O_5/ZrO_2 and V_2O_5/SiO_2 catalysts [28]. It has been reported that the reactivity in partial oxidation reactions is related to the reducibility of the VOx species on the support, and this is enhanced over ZrO_2 compared with SiO_2 [29]. V species supported on ZrO_2/SiO_2 interact preferentially with ZrO_2, but their behavior is different than on pure ZrO_2. Previous studies of the catalytic properties of VOx/ZrO_2/SiO_2 materials also demonstrated that the addition of vanadium atoms enhances the reactivity of pure ZrO_2/SiO_2 supports in oxidative dehydrogenation of butane [10].

It seems possible that a catalyst could be tailored to produce more dehydrogenation products, more partial oxidation products, or both. The balance between dehydrogenation activity and partial oxidation activity could fundamentally determine the product distribution as well as the possibility of further reactions, such as Diels–Alder. This work explores the effect of the level of acidity and the reducibility of V on the product distribution (cis-2-butene, trans-2-butene, butadiene, 3-cyclohexene-1-carboxaldehyde, benzaldehyde) during ODH of n-butane through changes in the ZrO_2 loadings on SiO_2.

We employed the use of grafting as a synthesis method to prepare a material consisting of highly dispersed zirconia over SiO_2, in order to obtain an acidic material with a higher surface area than pure ZrO_2. With ZrOx/SiO_2 supports, it is possible to obtain a better dispersion of vanadia than in pure SiO_2. The vanadia also provides redox sites for the oxidation reactions. In this manner, the redox properties of vanadia and the acidity of zirconia could be combined in the same material and have the potential to be selective for the production of butadiene and acrolein, necessary as reactants in the Diels–Alder reaction to produce benzaldehyde (Scheme 2).
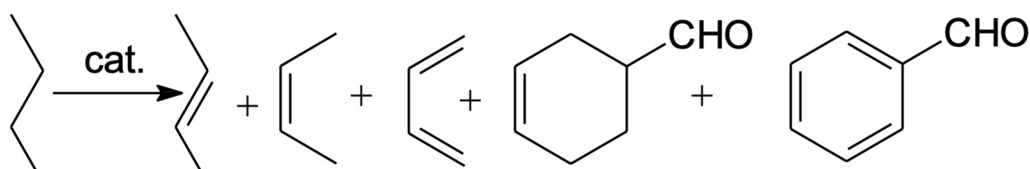
Scheme 2. Products formed from butane dehydrogenation and Diels-Alder reactions.

2. Results and Discussion

2.1. Textural Properties and VOx Structure

X-ray diffraction (XRD) patterns for ZrOx/SiO_2 and VOx/$yZrO_2/SiO_2$ materials ("y" represents the wt % of Zr loading) are shown in Figures 1 and 2, respectively. The results clearly indicate the presence of tetragonal ZrO_2 crystals at 25 wt % Zr loading, evidenced by diffraction peaks at $2\theta = 30°$, $50°$, and $60°$. This occurs at a somewhat lower level than the determined theoretical monolayer capacity. Crystalline phases are absent for Zr loadings of 20 wt % and lower, indicating a highly-dispersed ZrO_2 monolayer or perhaps patches of this structure coating the amorphous silica surface (broad 20–22° peak). Pothirat et al. [30] used a different Zr impregnation method and detected the formation of crystalline ZrO_2 with Zr loadings as low as 2 wt %, albeit with a SiO_2 support of considerably lower surface area than the one used here. The addition of 4 wt % V appears to promote the formation of tetragonal ZrO_2 crystals at lower Zr loadings, with the appearance of these peaks already at 20 wt % Zr (Figure 2). No crystalline phases are detected in the XRD of VOx/10ZrOx/S, yet interestingly enough, very weak broad tetragonal ZrO_2 peaks appear with VOx/5ZrOx/S. Given the low V loadings used in these samples, it is unlikely that V_2O_5 or ZrV_2O_7 phases would be detectable with XRD, and it is

significant that the Raman data (see below) clearly show evidence of crystalline V_2O_5 and ZrV_2O_7 in the VOx/5ZrOx/S and VOx/10ZrOx/S catalysts.
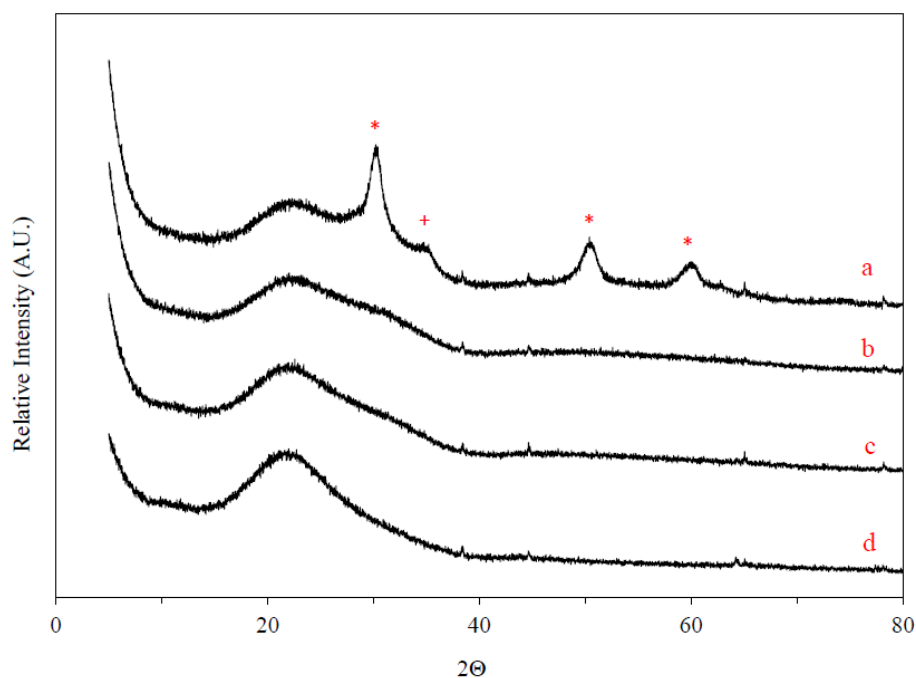

Figure 1. X-ray diffraction (XRD) patterns: (**a**) 25ZrOx/S, (**b**) 20ZrOx/S, (**c**) 10ZrOx/S, and (**d**) 5ZrOx/S. (*) ZrO_2, (+) $ZrSiO_4$.
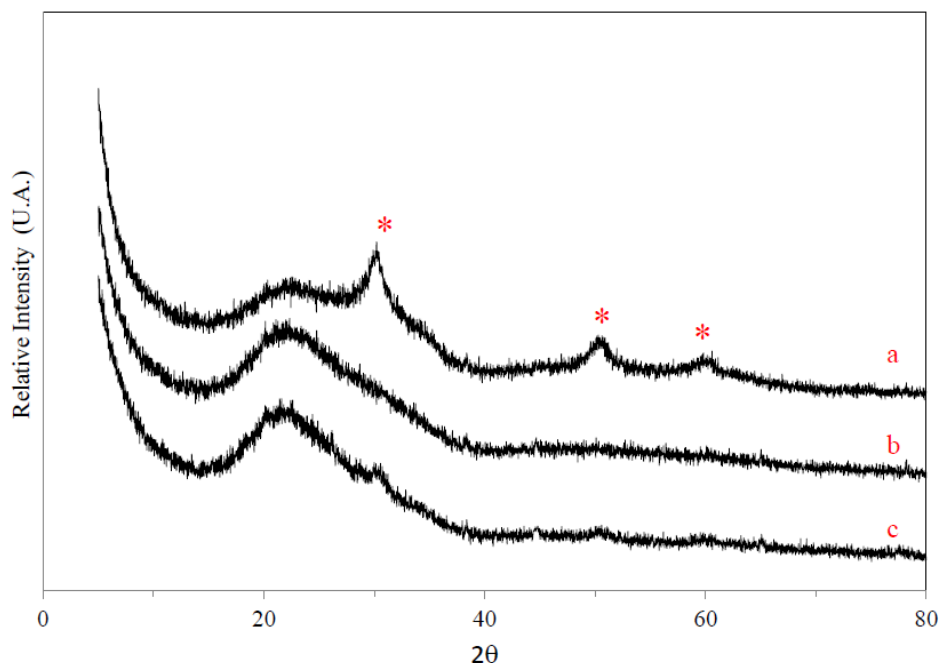

Figure 2. XRD patterns of VOx/yZrOx/S: (**a**) VOx/20ZrOx/S, (**b**) VOx/10ZrOx/S, and (**c**) VOx/5ZrOx/S. (*) ZrO_2.

Nitrogen physisorption of all materials shows that the formation of crystalline species results in a loss of surface area (see Table 1). For vanadium-free samples, there is not a large change of surface area for 5 wt %–20 wt % Zr; however, the areas are significantly smaller than that of the pure silica. The surface area reduction notably decreases with 25 wt % Zr to 269 m^2/g. The BET areas of the

vanadium-modified materials are all smaller than the corresponding Zr-modified silica, and similar to the surface area of 25ZrOx/S. All samples were found to be non-microporous.

Table 1. BET surface area in synthesized catalysts.

Catalyst	BET Area (m^2/g)
S [1]	380
1VOx/S	-
2VOx/S	-
5VOx/S	266
VOx/ZrO$_2$	89
5ZrOx/S	336
10ZrOx/S	344
20ZrOx/S	320
25ZrOx/S	269
VOx/5ZrOx/S	251
VOx/10ZrOx/S	239
VOx/20ZrOx/S	266

[1] S refers to the SiO$_2$ support (Aerosil).

The Raman spectra of dehydrated samples (VOx/20ZrOx/S, VOx/10ZrOx/S, VOx/5ZrOx/S, 5VOx/S, 2VOx/S, and 1VOx/S) are shown in Figure 3. Published band assignments for pure silica appear at 410, 487, 607, 802, and 976 cm^{-1} [29]. The Raman spectra of 2VOx/S and 1VOx/S materials are very similar, showing the vanadyl stretch band (V = O) between 1000 and 1050 cm^{-1} (maximum at 1035 cm^{-1}), a very weak broad feature at 920 cm^{-1}, and a band at 266 cm^{-1}. The low vanadium loadings used here (0.4–0.8 V/nm^2) favor the formation of isolated tetrahedral VO$_4$ species on silica, and the vanadyl stretch (1035 cm^{-1}) band intensifies with increased V loading [29]. The 920 and 266 cm^{-1} features may imply the presence of a small amount of polymeric VOx species, these bands being associated with stretch and bending modes of V–O–V linkages [31]. In the 5VOx/S sample, the vanadium has agglomerated to form crystalline V$_2$O$_5$, with Raman bands detected at 144, 195, 285, 303, 405, 481, 528, 701, and 996 cm^{-1}. These results clearly show that, on pure Aerosil 380 support, increasing vanadium loading from 2 wt % to 5 wt % leads to the formation of nanocrystalline V$_2$O$_5$, which were undetected by XRD. In the zirconia-containing samples VOx/5ZrOx/S and VOx/10ZrOx/S, V$_2$O$_5$ nanocrystals are present even at 4 wt % vanadium content with V$_2$O$_5$ Raman bands located as reported for 5VOx/S, though several appear convoluted with emerging bands owing to the Zr addition. The Raman evidence for exposed silica surface is not clear from the spectra of either VOx/5ZrOx/S or VOx/10ZrOx/S, although the 481 and 529 cm^{-1} V$_2$O$_5$ bands appear to be convoluted with the broad silica band located at 487 cm^{-1}. A Raman band appearing near 775 cm^{-1} in VOx/10ZrOx/S and VOx/20ZrOx/S can be attributed to nanocrystalline ZrV$_2$O$_7$ [32]. The emergence of small amounts of nanocrystalline tetragonal ZrO$_2$ is implied by weak bands appearing at 650 cm^{-1} and distortion of the 481 cm^{-1}, 285 cm^{-1}, and 303 cm^{-1} V$_2$O$_5$ bands. Both VOx/5ZrOx/S and VOx/10ZrOx/S show weak, but distinct vanadyl stretch bands located between 1020 and 1035 cm^{-1}, indicative of a small amount of vanadium associated with monovanadate species, probably on amorphous or nanocrystalline zirconia patches.
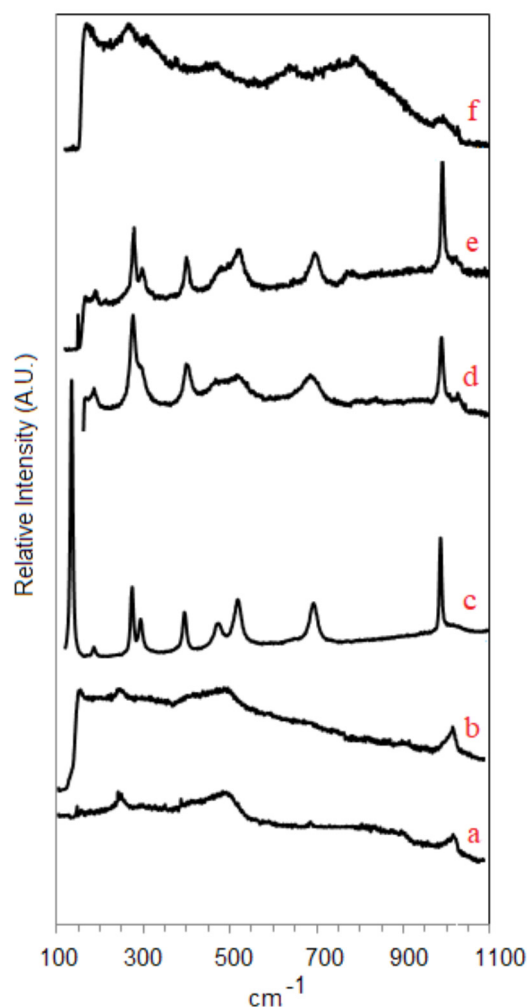
Figure 3. Raman shift: (**a**) 1VOx/S, (**b**) 2VOx/S, (**c**) 5VOx/S, (**d**) VOx/5ZrOx/S, (**e**) VOx/10ZrOx/S, and (**f**) VOx/20ZrOx/S.

In VOx/ZrO$_2$ catalysts with comparable V loadings, both monovanadate and polyvanadate VOx may be present, although, except for the 775 cm^{-1} band mentioned for VOx/10ZrOx/S, our spectra do not show distinct features in the 800–950 cm^{-1} region expected for polyvanadates on pure zirconia. The presence of V$_2$O$_5$ species in VOx/5ZrOx/S and VOx/10ZrOx/S gives a clear indication that zirconia coverage of the silica support is incomplete: at a sub-monolayer Zr loading, vanadium grafting on bare silica makes likely the agglomeration of these species to V$_2$O$_5$ crystals with thermal treatment. At higher Zr loadings, there is a more extensive ZrO$_2$ overlayer, and hence more grafting of V species on ZrO$_2$, where the stronger affinity (relative to silica) results in a more stable, amorphous vanadia overlayer on amorphous (or crystalline) zirconia. As the XRD results have shown for the 20 and 25 wt % Zr samples, ZrO$_2$ crystallization appears to be promoted by vanadium. The Raman technique is more sensitive than XRD at detecting nanocrystalline tetragonal ZrO$_2$ and ZrV$_2$O$_7$ at these low metal contents, thus showing that V is already interacting with Zr at 5 wt %–10 wt % zirconium content. Gazzoli et al. [33,34] detected only the presence of polymeric vanadia species in VOx/ZrO$_2$ catalysts prepared from aqueous solutions at low loadings (2.7 wt %), although crystalline V$_2$O$_5$ and ZrV$_2$O$_7$ were found to co-exist with the dispersed species at higher V loadings. They confirmed this with atomic force microscopy, showing that the morphology of vanadium supported on zirconia changes with vanadium content from a smooth to a granular surface, where only a fraction of vanadium interacts directly with the zirconia and the rest forms two- and three-dimensional vanadium structures. The VOx/20ZrOx/S sample shows distinct

Raman bands at 317, 463, and 649 cm^{-1} that are characteristic of tetragonal ZrO$_2$ [29]. The broad 450–490 cm^{-1} band and the bands on 230, 360, and 975 cm^{-1} may indicate the presence of Zircon (ZrSiO$_4$) [29]. The VOx structure of this catalyst is devoid of V$_2$O$_5$ crystals. The very broad band structure between 700 and 900 cm^{-1} can be associated with the V–O–V vibrations of polyvanadate species, as reported by Su and Bell for VOx/ZrO$_2$ [35]. The bending mode of this group may be responsible for the poorly-defined band at 270 cm^{-1}, as V-O-V species have been reported to have deformation bands between 200 and 300 cm^{-1} [29]. Another broad region, from 980 to 1040 cm^{-1}, refers to the vanadyl stretches, implying a distribution of polymeric VOx sites. The weak band centered at 1033 cm^{-1} refers to the presence of a small density of isolated VO$_4$ species. The high resolution transmission electron microscopy (HRTEM) annular dark field image (Z-contrast) of the VOx/10ZrOx/S catalyst shown in Figure 4 documents the presence of 2–3 nm sized ZrO$_2$ and V$_2$O$_5$ nanophases decorating the Aerosil 380 structure. A more profound characterization of these structures was beyond the scope of this study, yet this evidence affirms that discrete Zr and V phases are in close proximity to each other and suggest synergistic behavior for catalysis involving acidic and redox sites.
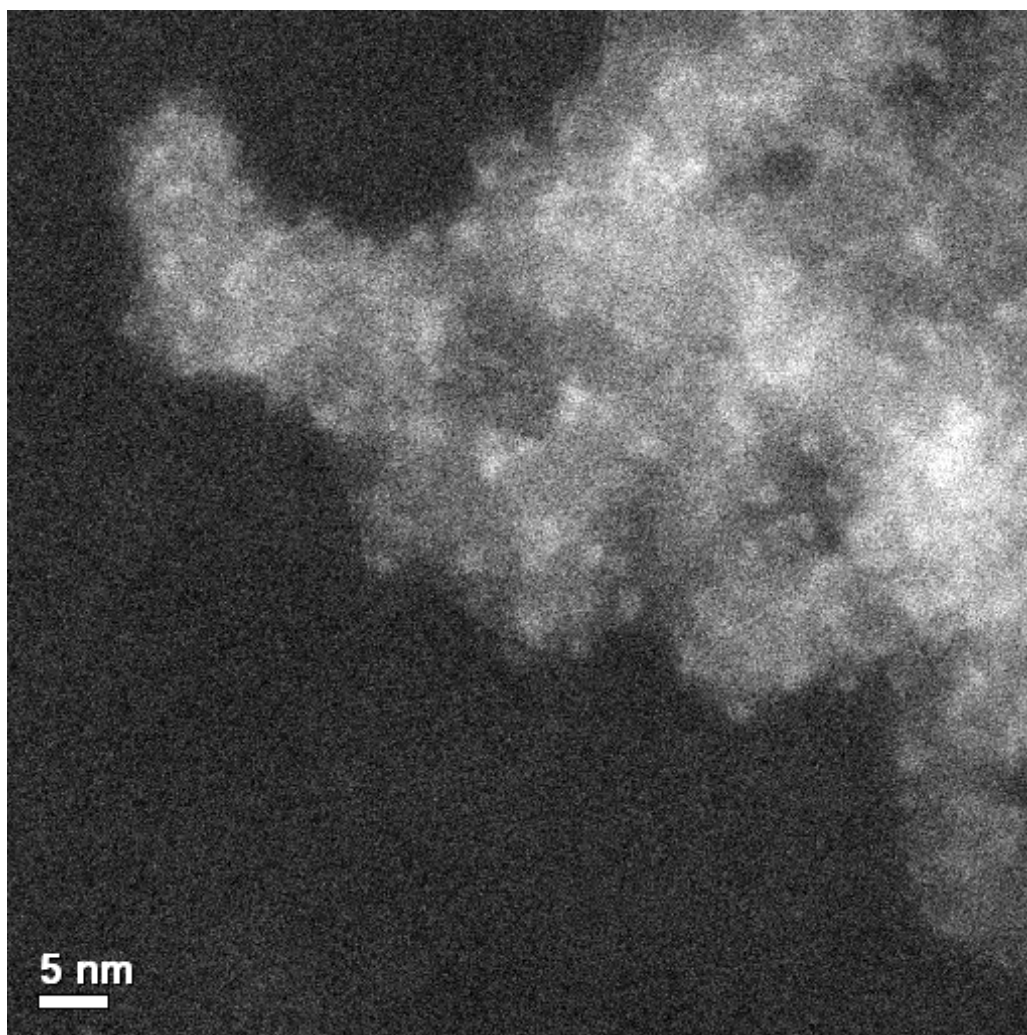

Figure 4. Annular dark field micrograph of the VOx/10ZrOx/S catalyst.

Figure 5 presents an overview of the type and coverage of zirconia and vanadia species distributed on the silica surface of the studied samples. Even at the low V loadings used here (V/nm^2 = 2.0), vanadium that grafts on pure or exposed silica surface agglomerates into V$_2$O$_5$ nanocrystals (VOx/5ZrOx/S and VOx/10ZrOx/S) upon calcination. In the cases of VOx/5ZrOx/S

and VOx/10ZrOx/S, most of the vanadia agglomerates to form V_2O_5 nanocrystals after calcination. At sub-monolayer coverages (≤10 wt % Zr), zirconia exists first as isolated 2D amorphous islands, to which the vanadium precursor molecule grafts directly to form a stable overlayer of monomeric VOx that resists agglomeration, given the stronger vanadia–zirconia interaction versus vanadia–silica. With increasing Zr content, the amorphous zirconia overlayer co-exists with 2–3 nm ZrO_2 nanocrystals of tetragonal phase. V grafting to these structures forms VOx/t-ZrO_2 and ZrV_2O_7 nanostructures with thermal treatment. At 20 wt % Zr, tetragonal ZrO_2 nanocrystals and amorphous material completely cover the silica surface, resulting in a diversity of monovanadate and polyvanadate monolayer species, rather than crystalline V_2O_5.
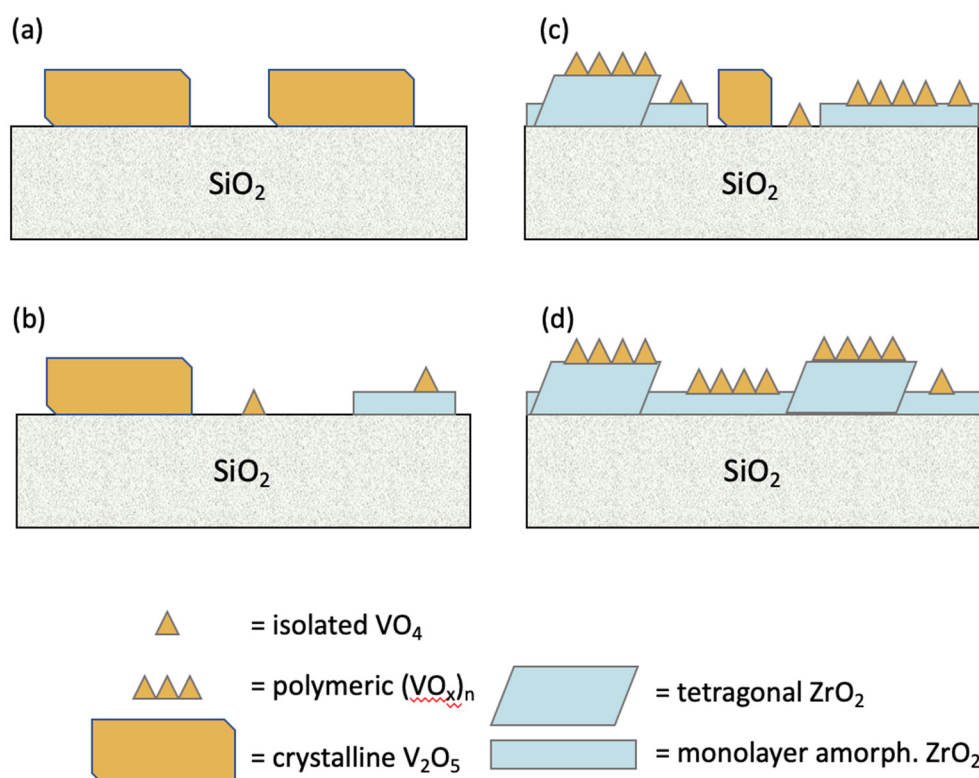

Figure 5. Proposed zirconia and vanadia structures. (**a**) 5VOx/S, (**b**) VOx/5ZrOx/S, (**c**) VOx/10ZrOx/S, and (**d**) VOx/20ZrOx/S.

2.2. Acidity

The pure silica support is only weakly acidic, and the addition of zirconia to the silica imparts Lewis acidity to the mixed oxide support. Site energy distribution histograms, obtained with NH_3 adsorption microcalorimetry, are displayed for ZrO_2-SiO_2 and VOx/$yZrO_2$/SiO_2 samples in Figure 6. It is observed that, in the ZrO_2-SiO_2 supports, the surface density and strength of the acid sites increases with increasing Zr content. In particular, site densities for sites in the 120–140 kJ/mol range increased, from 20 µmol/g (VOx/5ZrOx/S) to 80 µmol/g (VOx/20ZrOx/S). The site densities of the weakest sites, 60–80 kJ/mol, attributable to weakly acidic silica surface [36,37], practically disappear in 20ZrOx/S, suggesting that the Zr content achieves monolayer coverage, an indication that the ammonia adsorbs only on Zr sites on this sample. The calorimetric measurements thus give a reliable measure of the extent by which zirconia covers the silica surface. Medium strength acid sites (80–100 kJ/mol) also increase with Zr content. The acid site strengths measured are within the range reported in the literature for ZrO_2 supported on silica [37].
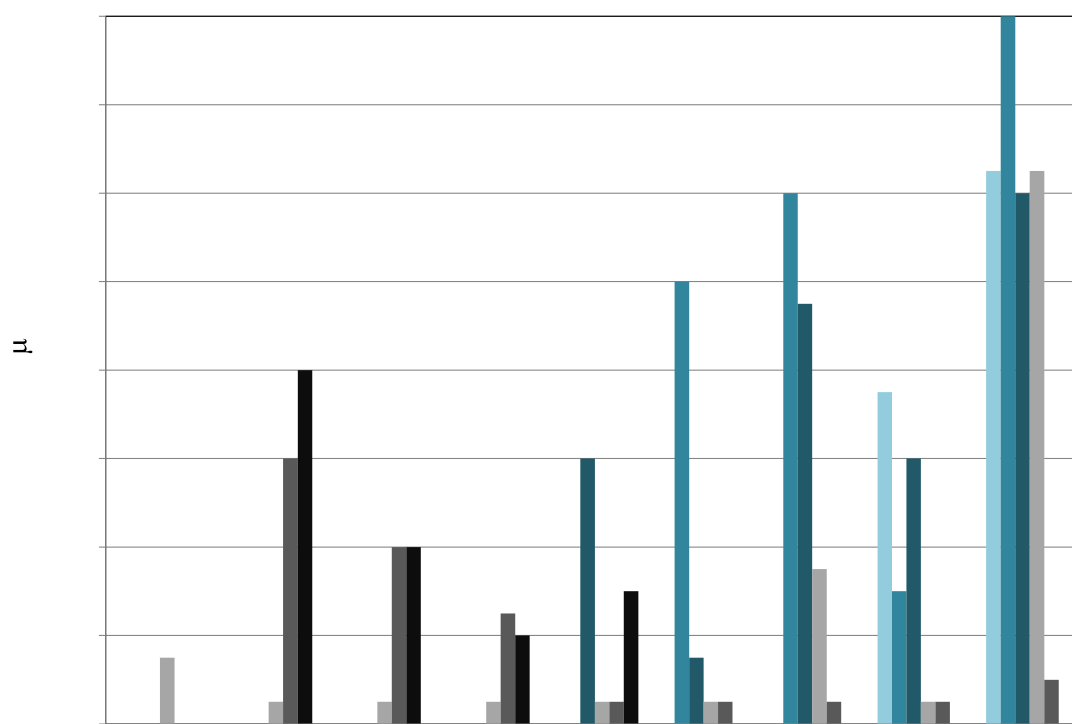
Figure 6. Differential heat of NH$_3$ adsorption on yZrOx/S and VOx/yZrOx/S samples: ■—5ZrS, ■—10ZrS, ■—20ZrS, ■—VOx/5ZrS, ■—VOx/10ZrS, ■—VOx/20ZrS.

The addition of vanadium to the ZrO$_2$-SiO$_2$ supports suppresses the strongest acid sites (strengths above 100 kJ/mol), while the density of sites corresponding to the 60–100 kJ/mol range increase with this process in all three samples (5 wt %, 10 wt %, and 20 wt % Zr). The VOx/5ZrOx/S catalyst has a predominantly silica exposed surface, and hence more "silica-like" behavior than the higher zirconia coverage in VOx/10ZrOx/S, which possesses a higher density of stronger acid sites in the 80–100 kJ/mol range. These stronger sites can be associated with the well-dispersed, amorphous VOx-ZrO$_2$ layer structure that likely forms V–O–Zr linkages, rather than with V–O–Si or V$_2$O$_5$, which typically shows only weak NH$_3$ adsorption. In the case of VOx/20ZrOx/S, with the most developed nanocrystalline tetragonal ZrO$_2$ structures, the total acid site density is slightly less than with VOx/10ZrOx/S, and this may refer to the more complete coverage of the zirconia surface by polymeric V species supported on ZrO$_2$ crystals, although the site strengths are comparable. Chary et al. [38] found that in VOx/ZrO$_2$, the formation of V$_2$O$_5$ crystals occurred if the V content was above a theoretical monolayer over the ZrO$_2$, and at this point, the acidity decreased. It is clear from these observations that vanadium-free exposed zirconia surface generates the strongest acid sites (greater than 120 kJ/mol NH$_3$ adsorption heat). In summary, the interaction of vanadium with zirconia species results in medium to low strength sites (between 80 and 100 kJ/mol), although the total acid site density is much higher than without the vanadia. Sites generated with 60 kJ/mol or below formed after V grafting relate to the adsorption of NH$_3$ on bare silica and V$_2$O$_5$ crystallites [36,39] and have little consequence for catalytic function.

2.3. Reducibility

Temperature programmed reduction (TPR) profiles shown in Figure 7 document V reducibility in 5VS, VOx/5ZrOx/S, VOx/10ZrOx/S, and VOx/20ZrOx/S catalysts, as crystalline ZrO$_2$ and zirconia supported on silica are not reducible [29,33]. The reduction of the silica-supported V$_2$O$_5$ crystallites (5VS) took place between 723 K and 973 K in a single peak, centered at 857 K, in agreement with

vanadium reducing from V^{5+} to V^{3+} (Table 2). Single reduction peaks were also registered for the other catalysts.
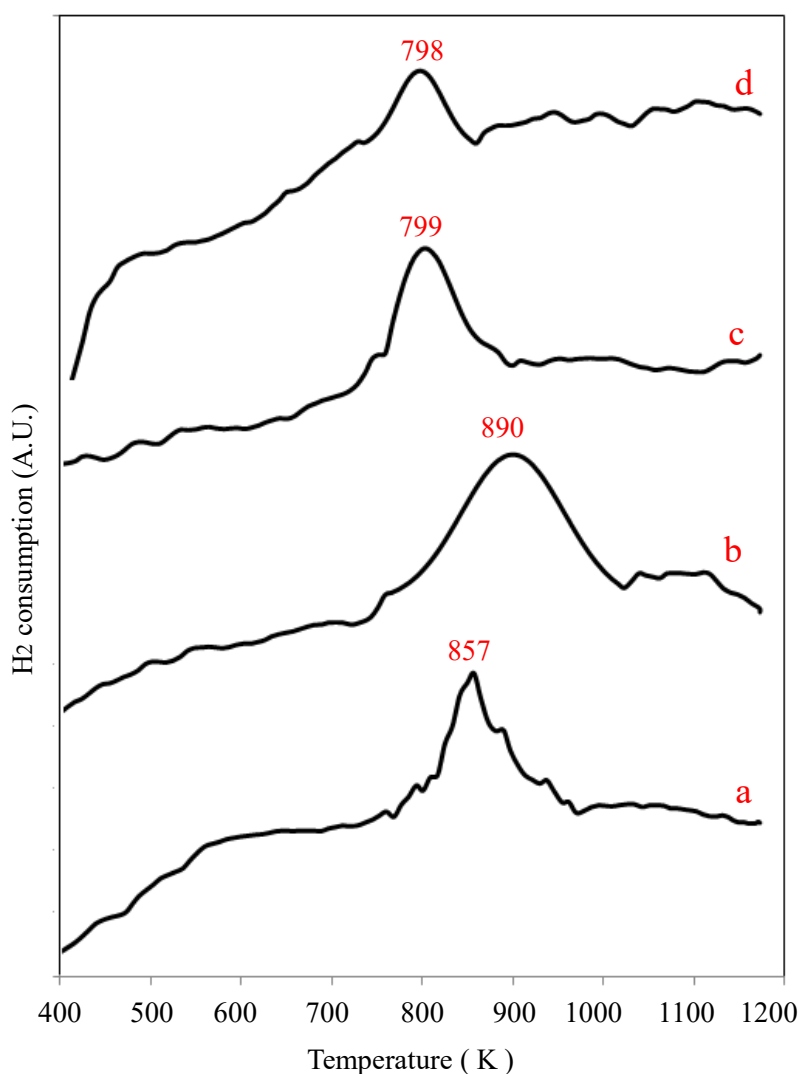

Figure 7. TPR profile of various VOx/yZrOx/S catalysts: (**a**) 5VOx/S, (**b**) VOx/5ZrOx/S, (**c**) VOx/10ZrOx/S, and (**d**) VOx/20ZrOx/S.

Table 2. Comparison of TPR results for VOx on different supports and the theoretical and experimental H_2 consumption. T_{max} corresponds to the temperature of maximum H_2 consumption.

Catalyst	V (mg)		Theoretical H_2 Uptake ($\mu mol\ H_2$)			Experimental H_2 Uptake ($\mu mol\ g^{-1}$)
		T_{max} (K)	$V^{5+} \rightarrow V^{4+}$	$V^{5+} \rightarrow V^{3+}$	$V^{5+} \rightarrow V^{2+}$	
5VOx/S	5.21	857	28.7	57.3	86.0	58
VOx/5ZrOx/S	4.06	890	22.4	44.7	67.1	43.5
VOx/10ZrOx/S	3.82	799	21.0	42.0	63.1	22
VOx/20ZrOx/S	3.88	798	21.3	42.7	64.0	8.3

For VOx/5ZrOx/S, the reduction peak is wider than for 5VOx/S, and T_{max} is displaced to a higher temperature (890 K). This suggests the presence of different VOx species on the surface, however, the hydrogen consumption shows that they undergo similar changes of oxidation state (V^{+5} to V^{+3}).

As mentioned earlier, the Raman results show evidence for the presence of V_2O_5 crystallites and a small amount of monovanadates in this sample. The reduction of the monovanadates on ZrO_2 could be responsible for shifting the T_{max} to higher temperatures. As has been reported in other works, the TPR profiles shift positions depending on the vanadium content. The reduction of monovanadates occurs at higher temperatures than small polyvanadate aggregates, and peak maximum temperatures as high as 800 K have been reported for the monovanadates reduction [40,41]. At higher Zr content, the V reduction profiles shift to lower temperatures, with T_{max} being nearly the same for VOx/10ZrOx/S and VOx/20ZrOx/S, which is typical of TPR results with materials supported on SiO_2 modified with increasing amounts of zirconia, where the reduction temperature of VOx decreases with the increment of the Zr loading [29]. The degree of V reduction, however, is considerably lower with our samples with more Zr, owing either to a lower reduction stoichiometry or to some vanadia becoming inaccessible because of an association with zirconia. In the case of VOx/10ZrOx/S, stoichiometry would agree with V reducing only to 4+, but the low experimental H_2 uptake with VOx/20ZrOx/S implies that a considerable portion of V^{5+} does not reduce at all.

2.4. Catalytic Activity Oxidative Dehydrogenation (ODH) of n-Butane

The reaction was monitored for several hours until the system reached stability (three hours). The microactivity results for all the catalysts showed selectivity to dehydrogenation and oxidation products (see Table 3), while only VOx/5ZrOx/S and VOx/10ZrOx/S had selectivity to benzaldehyde. The partial oxidation products were detected via gas chromatography-mass spectrometry GC-MS, although they were not quantified. Acrolein was produced in all of the catalysts except for VOx/ZrO_2. The most active catalyst, VOx/10ZrOx/S, was also the most selective to dehydrogenation products.

Table 3. Butane conversion (X butane) and selectivity (S_i) to butane oxidation and dehydrogenation products observed with the different catalysts.

Catalyst	$X_{n\text{-butane}}$ (%)	$S_{butadiene}$ (%)	$S_{cis\text{-}2\text{-}butene}$ (%)	$S_{trans\text{-}2\text{-}butene}$ (%)	$S_{1\text{-}butene}$ (%)	$S_{benzaldehyde}$ (%)	S_{CO} (%)	S_{CO2} (%)	Cx [1] (%)
VOx/5ZrOx/S	4	20	0	0	0	29	38	7	6
VOx/10ZrOx/S	15	44	3	3	0	20	6	7	17
VOx/20ZrOx/S	5	25	10	7	0	0	30	21	6
VOx/ZrO_2	11	7	24	22	20	0	8	14	0

[1] Cx = partial oxidation products.

The incorporation of Zr and V by the grafting method leads to different VOx structures. These structures are influenced by the presence of Zr and Si environments and reflect three catalytic functions, namely, dehydrogenation, partial oxidation, and complete oxidation, and the relative activities of different VOx structures and their active sites based on acidity and redox behavior.

Several authors have studied the role of surface acidity and redox properties for the activation of hydrocarbons. Mechanistically, acid sites are essential for activating the alkane reactant molecule to form ODH products, although a considerably higher acid site strength and density will undesirably oxidize ODH intermediate molecules and also provide a direct reaction path to oxidation products. Incorporation of vanadia in the ZrO_2/SiO_2 matrix used here greatly diminished the acid strength of exposed zirconia. As the experimental results show, the activation of butane can occur even on very weak acid sites. Vanadium addition blocks the strongest Lewis acid sites present in dispersed zirconia, replacing them with weaker sites still capable of activating n-butane.

VOx/10ZrOx/S has the largest number of total acid sites and the highest conversion is observed with this material. However, VOx/20ZrOx/S has acidity with medium strength (80–100 kJ/mol) that is not very different (100 vs. 75 µmol/g), but the conversion observed with this material is about one-third of that for VOx/10ZrOx/S. Using T_{max} from TPR as an indicator of V reducibility, VOx/10ZrOx/S and VOx/20ZrOx/S are similar in this regard, but the number of reducible sites in the latter (22 µmol H_2 consumed g^{-1}) is about one-third of that in the former (8.26 µmol H_2 consumed g^{-1}), mirroring

the activity. The very weak acid sites in VOx/5ZrOx/S (acid strength < 70 kJ/mol) stemmed largely from V_2O_5 crystallites that are also not easily reducible (T_{max} = 890 K), which may explain the low conversion observed with this material.

Therefore, acidity alone cannot explain differences in catalytic activity. Activation of butane thus requires more easily reducible vanadia and at least medium strength acid sites.

It would be expected that, at higher conversions, the selectivity to CO and CO_2 should be higher. Interestingly, in this study, the highest conversion (15%) was observed with VOx/10ZrOx/S, the catalyst that shows the lowest formation of COx, suggesting that its surface does not favor complete oxidation reactions.

Of the three materials, only VOx/20ZrOx/S has relatively strong acid sites, with 50 µmol/g of 90–110 kJ/mol NH_3 adsorption strength, which are absent in the other catalysts, where the selectivity to CO_2 is significantly lower (7% vs. 21%). Thus, acidity seems to be the only factor that determines to which extension CO_2 is formed over the studied materials. To confirm it, additional experiments were performed with a ZrO_2 catalyst, where the acidity was not moderated by the presence of vanadia. In this case, only strong acid sites were observed (>100 kJ/mol) and the conversion of butane to CO_2 was above that observed with the materials reported here. Summarizing, for materials with similar reducibility of V, the selectivity to CO_2 is controlled only by acidity.

If acidity is moderated, partial oxidation products should be favored over CO_2 formation. Acrolein is clearly formed over the catalysts that produced benzaldehyde (VOx/5ZrOx/S, VOx/10ZrOx/S), which have lower acid strength and more reducible sites.

Acidity and reducibility seem to also play an important role in the dehydrogenation activity of each catalyst. Regardless of the site density or strength, all the catalysts were active for the dehydrogenation function. Reaction tests with VOx/SiO$_2$ performed separately showed not only low conversion (4%), but very low activity to dehydrogenation (3% selectivity to butadiene), and the most abundant products were CO and CO_2, showing that dehydrogenation requires an acidic catalyst.

The predominant ODH product was 1,3-butadiene in all three catalysts and the appearance of 2-butenes may be related to the existence of weaker acid sites than those that favor the formation of CO_2. The only materials that show benzaldehyde formation are VOx/5ZrOx/S and VOx/10ZrOx/S, and it is interesting to note that their acidity is more moderated than for VOx/20ZrOx/S, which in addition is the one with less reducible sites. The amount of butane that undergoes dehydrogenation is responsible for the yields of butenes, butadiene, and (with consecutive reaction) benzaldehyde. The combined selectivity to these compounds observed in the microactivity studies is higher over the materials with medium to low acidity. In the absence of strong acid sites, the generated dehydrogenation products will not undergo oxidation reactions and their yield correlates with the number of sites of medium strength (60–90 kJ/mol), rendering VOx/10ZrOx/S as the most active material.

Gazzoli et al. 2009 [33] did not detect any formation of butadiene with catalysts based on vanadium supported on zirconia; they only reported selectivity to cis- and trans-2-butenes that were associated with the presence of vanadium polymeric species. In our study, butadiene is formed in important amounts over all three catalysts, but only with VOx/20ZrOx/S were there polymeric VOx species detected with Raman spectroscopy, while in the other two catalysts, the VOx was found to be monovanadate.

According to our results, the presence of silica modifies the interaction between Zr and V, perhaps owing to the monolayering of zirconia and vanadia via the grafting method, and the polymeric VOx species behave differently, with the results showing a low selectivity to butenes, yet important selectivity to 1,3-butadiene. According to Chen et al. 2000 [42], the essential requirements for a selective ODH catalyst are intermediate reducibility, weak Lewis acid centers, and high oxygen mobility. In this regard, the higher activity of VOx/10ZrOx/S catalyst with reasonable ODH selectivities to butenes and butadiene represents the proper compromise among these factors.

The formation of benzaldehyde in a Diels–Alder reaction between the butadiene and the acrolein may occur in a homogeneous or heterogenous mechanism. Some other authors [43] have reported the

presence of aromatic compounds on the oxidation of n-butane. They have associated these structures to a Diels–Alder mechanism between the butadiene oxidation product (maleic anhydride), formed over vanadium catalysts, and some unsaturated compounds [43–45]. It might be possible that vanadium generates the catalytic sites for this reaction owing its redox properties.

The presence of benzaldehyde in our results as well as the traces of other aromatic compounds indicates that a Diels–Alder reaction takes place over the catalysts in tandem with the dehydrogenation and oxidation reactions. For dehydrogenation reactions and partial oxidation reactions, to produce enough diene (butadiene) and acrolein (dienophile) requires medium strength acidity and enough reducible sites. The product formed, 3-cyclohexene-1-carboxaldehyde, on a surface like this will undergo further dehydrogenation to produce benzaldehyde.

3. Materials and Methods

3.1. Catalyst Synthesis

Vanadium and zirconium were grafted onto silica support (Aerosil Degussa, 380 m^2/g) in a two-step procedure. The grafting method consisted of the controlled hydrolysis between support hydroxyl groups and metal alkoxide precursor molecules. In the first step, the Zr alkoxide amounts were adjusted in order to obtain ZrO_2/SiO_2 supports with 5 wt %, 10 wt %, 20 wt %, and 25 wt % Zr content. Initially, the silica was placed in a round-bottomed flask and pre-dried at 473 K for 3 h under flowing oxygen, after which the gas flow was switched to argon and cooled to room temperature. Sufficient toluene (J.T. Baker, AR grade, Waltham, MA, USA) was added to cover the silica support. An appropriate amount of zirconium (IV) n-butoxide (Aldrich, 80%) was then added, and the flask contents were continuously stirred at room temperature for 12 h under inert gas flow. Contents were kept under reflux to avoid toluene evaporation losses. Finally, the solid was filtered and washed with fresh solvent, dried at 373 K, and calcined in flowing oxygen at 673 K for 8 h. In the second step, catalysts in their final form were prepared by grafting vanadyl (V) triisopropoxide (98%, Alfa-Aesar, Tewksbury, MA, USA) onto the ZrO_2/SiO_2 materials to achieve 4 wt % V loading. This V grafting step was analogous to the one outlined earlier for Zr, although using isopropanol as the solvent and a hydrolysis temperature of 333 K. Catalysts were calcined at 823 K for 8 h prior to testing.

For Raman spectroscopy, VOx/SiO_2 reference materials were prepared by the incipient wetness impregnation of V on silica, using aqueous solutions of ammonium metavanadate-oxalic acid (1:2 ratio) with concentrations adjusted to give 1 wt %, 2 wt %, and 5 wt % of V loadings. These samples were dried at 393 K, and calcined at 823 K in flowing oxygen for 8 h. Catalyst designations as well as V and Zr content are provided in Table 4.

Table 4. V and Zr loadings in synthesized catalysts.

Catalyst	wt % Zr	wt % V
S [1]	0	0
1VOx/S	0	1
2VOx/S	0	2
5VOx/S	0	5
VOx/ZrO_2	-	4
5ZrOx/S	5	-
10ZrOx/S	10	-
20ZrOx/S	20	-
25ZrOx/S	25	-
VOx/5ZrOx/S	5	4
VOx/10ZrOx/S	10	4
VOx/20ZrOx/S	20	4

[1] S refers to the SiO_2 support (Aerosil).

3.2. Nitrogen Physisorption

Specific surface areas were determined with nitrogen adsorption isotherms at 77 K, using a homemade volumetric adsorption apparatus equipped with precision capacitance manometers (Baratron MKS Instruments, Inc., Andover, MA, USA) capable of achieving 10^{-6} Torr under dynamic pumping. Prior to obtaining the adsorption isotherms, samples were degassed (10^{-3} torr) at 473 K for 2 h in order to desorb any impurity or water on the surface. Brunauer-Emmett-Teller (BET) and t-plot analysis were conducted with at least ten points obtained in the 0.01–0.40 p/p_o range.

3.3. X-Ray Diffraction

Powder X-ray diffraction patterns were collected on a PANalytical X-ray diffractometer system model X'Pert PRO (Almelo, Netherlands), using Cu Kα radiation (λ = 0.15405 nm, 35 kV, 30 mA) and collecting data in the $5° < 2\theta < 80°$ range.

3.4. High Resolution Transmission Electron Microscopy (HRTEM)

HRTEM analysis was performed with a JEOL JEM-ARM200F (Peabody, MA, USA) operated in scanning transmission electron microscopy (STEM) mode (at 200 kV, 78 pm resolution) equipped with an EDS detector for elemental analysis.

3.5. Fourier-Transform Infrared Spectroscopy (FTIR)

In situ FTIR spectroscopy of pyridine adsorption experiments were performed with a Bruker Vector 22 FTIR spectrometer (Billerica, MA, USA) equipped with a Harrick "Praying Mantis" diffuse-reflectance cell with environmental chamber and KBr windows. Self-supported catalyst wafers were pre-treated in dry flowing nitrogen (200 cm^3/min) at 573 for 60 min, cooled to 323 K, saturated by injection of pyridine into the nitrogen flow, and analyzed after degassing.

3.6. Ammonia Adsorption Microcalorimetry

Adsorption calorimetry was conducted on a homemade Tian–Calvet calorimeter (San Luis Potosí, SLP, Mexico) at 473 K, whose construction and operation are described in [46]. In brief, 0.2 g sample sizes were previously degassed under vacuum (10^{-5} torr) at 673 K to achieve a leak rate no greater than 10^{-4} torr/min at that temperature, before inserting the cells in the calorimeter and stabilizing the heat flow baseline. Ammonia gas doses of 10 µmol/g were admitted in succession onto the sample, allowing sufficient time (ca. 45 min) for each dose to achieve thermal equilibrium before proceeding with the next dose. This procedure was continued up to a saturation pressure of at least 3 torr NH_3, obtaining both isotherm and differential heat of adsorption data. The differential heat plot data in turn were analyzed, using a procedure reported by Shen et al. [47], to obtain site energy distribution histograms for comparing samples. For acidity comparison purposes, this range starts with NH_3 adsorption energies of 60 kJ/mol and higher.

3.7. Temperature Programmed Reduction (TPR)

TPR runs were conducted with 100 mg of samples, ground and sieved to 0.1–0.3 mm size, and loaded into a quartz U-tube microreactor (4 mm ID). Samples were pre-oxidized at 823 K for 2 h in pure oxygen, with a flowrate of 100 cm^3/min at normal temperature and pressure (NTP). After this treatment, the samples were cooled to room temperature, the gas flow was switched to a reducing gas (5% H_2/Ar, 30 cm^3 NTP/min), and then heated at 10 K/min to 1173 K. Hydrogen consumption was measured online using a gas chromatograph (Chromepak MicroGC equipped with CPSil 5 and Hayesep A columns and a thermal conductivity detector (Raritan, Franklin, NJ, USA), using argon as the reference carrier gas.

3.8. Raman Spectroscopy

Raman spectra were obtained with a Jobin-Yvon-HORIBA T64000 micro-analysis system (Kyoto, Japan), equipped with a triple-pass monochromator and a CCD photodiode array cooled to 140 K. Photo-excitation was accomplished with the 514.5 nm line of an Ar^+ laser (Spectra Physics, model 2017, Santa Clara, CA, USA) using 1.5 mW power focused to ca. 2.0 μm illumination diameter on powdered sample pellets (pressed to 179 bar) aligned in an optical stage of an Olympus (Model BH2-UMA, Shinjuku, Tokyo, Japan) microscope and objective lens (100X), through which the scattered radiation was collected and directed into the monochromator. Spectra were recorded by co-adding two accumulations of 30 s duration in the following ranges: 120–720 cm^{-1} and 720–1300 cm^{-1}.

3.9. Catalytic Activity

Microactivity measurements for the oxidative dehydrogenation of n-butane were performed with the same reactor system used for TPR measurements. Prior to reaction testing, 0.1 g of catalyst was treated for 2 h with flowing oxygen (100 cm^3 NTP/min) at 823 K. Immediately after this treatment, the reactor was cooled to 673 K and the reactor feed gas was adjusted to supply 90 cm^3 NTP/min of 5% O_2/He and 10 cm^3/min of n-butane. Under these conditions, conversions of 5% to 30% were achieved after a several hour period of stabilization. Both reactor feed and effluent streams were analyzed with the online GC system described above for TPR, but using pure helium as the reference gas. The GC system resolved dehydrogenation products (butenes, butadiene) as well as benzaldehyde, CO, and CO_2 for assessing both dehydrogenation as well as partial and total oxidation selectivity. After having reached steady-state, all the other compounds were identified from samples collected with a gas sampling bulb located at the reactor exit, and analyzed via GC-MS (Agilent Technologies Selective Mass Detector 5973 Network coupled with a 6890N GC). Butane conversion (X_{nC4} %) and selectivity to product i (S_i %) are reported according to the following equations:

$$X_{nC4} \% = (nC_4 \text{ consumed mol}/nC_4 \text{ initial mol}) \times 100$$

$$S_i \% = (\upsilon_{nC4}/\upsilon_i) (\text{product i mol}/nC_4 \text{ consumed mol}) \times 100$$

where υ_{nC4} and υ_i are the stoichiometric factors of n-butane and the product i, respectively, in the reaction of n-butane to product i.

4. Conclusions

The interplay between the molecules produced in dehydrogenation and partial oxidation reactions from butane lead to new products (via Diels-Alder) that have economic importance. The right balance between these competitive reactions depends on the level of acidity and the reducibility of the catalyst.

The addition of Zr induces acidity on SiO_2-based material with the number of sites and their strength increasing (up to 140 kJ/mol) with the zirconia loading 25ZrOx/S > 20ZrOx/S > 10ZrOx/S > 5ZrOx/S.

The grafting synthesis method is useful for achieving high dispersion of both vanadium and zirconium over the silica surface with zirconium concentrations up to theoretical monolayer coverage. Vanadium addition neutralizes the strongest acid sites present in dispersed zirconia, replacing them with weaker sites (<100 kJ/mol) still capable of activating n-butane. Vanadium preferentially interacts with the zirconium oxide supported on the silica surface, forming different structures depending upon Zr loading. TPR results show that V reducibility can be distinguished between "silica-like" and "zirconia-like" behavior, because low Zr coverage leaves a bare silica surface, allowing the formation of V_2O_5 crystals.

Slightly stronger acidity was observed with increasing Zr coverage, and these sites may be identified with polymeric VOx species, probably involving V–O–Zr linkages. ODH selectivity

differences were slight; the predominant ODH product was 1,3-butadiene in all three catalysts, and the appearance of 2-butenes may be related to the appearance of stronger acidity with V–Zr interaction.

The reducibility of the V decreased with increasing Zr loadings 20ZrOx/S < 10ZrOx/S < 5ZrOx/S and, in combination with strong acid sites, favored the formation of COx to the detriment of partial oxidation products.

Benzaldehyde is formed via a Diels–Alder reaction in a heterogeneous phase combined with the oxidative and dehydrogenation catalytic activity of the catalysts, where the higher yields corresponded to catalysts with monovanadate species characterized by medium acid strength sites and more easily reducible sites (T_{max} = 799 K).

References

1. Settle, A.E.; Berstis, L.; Rorrer, N.A.; Roman-Leshkóv, Y.; Beckham, G.T.; Richards, R.M.; Vardon, D.R. Heterogeneous Diels–Alder catalysis for biomass-derived aromatic compounds. *Green Chem.* **2017**, *19*, 3468–3492. [CrossRef]

2. Brühne, F.; Wright, E. Benzaldehyde. *Ullmann's Encycl. Ind. Chem.* **2000**. [CrossRef]

3. Choudhary, V.R.; Dhar, A.; Jana, P.; Jha, R.; Uphade, B.S. A green process for chlorine-free benzaldehyde from the solvent-free oxidation of benzyl alcohol with molecular oxygen over a supported nano-size gold catalyst. *Green Chem.* **2005**, *7*, 768–770. [CrossRef]

4. Choudhary, V.R.; Jha, R.; Jana, P. Solvent-free selective oxidation of benzyl alcohol by molecular oxygen over uranium oxide supported nano-gold catalyst for the production of chlorine-free benzaldehyde. *Green Chem.* **2007**, *9*, 267–272. [CrossRef]

5. Jia, A.; Lou, L.L.; Zhang, C.; Zhang, Y.; Liu, S. Selective oxidation of benzyl alcohol to benzaldehyde with hydrogen peroxide over alkali-treated ZSM-5 zeolite catalysts. *J. Mol. Catal. A Chem.* **2009**, *306*, 123–129. [CrossRef]

6. Marotta, R.; Di Somma, I.; Spasiano, D.; Andreozzi, R.; Caprio, V. Selective oxidation of benzyl alcohol to benzaldehyde in water by TiO_2/Cu (II)/UV solar system. *Chem. Eng. J.* **2011**, *172*, 243–249. [CrossRef]

7. Chevallier, M.L.; Dessolin, S.; Serres, F.; Bruyas, L.; Chatel, G. Effect of Ultrasound on the Green Selective Oxidation of Benzyl Alcohol to Benzaldehyde. *Molecules* **2019**, *24*, 4157. [CrossRef]

8. Bilyachenko, A.N.; Dronova, M.S.; Yalymov, A.I.; Korlyukov, A.A.; Shul'pina, L.S.; Arkhipov, D.E.; Shubina, E.S.; Levitsky, M.M.; Kirilin, A.D.; Shul'pin, G.B. Binuclear Cage-Like Copper (II) Silsesquioxane ("Cooling Tower")–Its High Catalytic Activity in the Oxidation of Benzene and Alcohols. *Eur. J. Inorg. Chem.* **2013**, *30*, 5240–5246. [CrossRef]

9. Figiel, P.J.; Kirillov, A.M.; Karabach, Y.Y.; Kopylovich, M.N.; Pombeiro, A.J. Mild aerobic oxidation of benzyl alcohols to benzaldehydes in water catalyzed by aqua-soluble multicopper (II) triethanolaminate compounds. *J. Mol. Catal. A Chem.* **2009**, *305*, 178–182. [CrossRef]

10. Sánchez-García, J.L.; García-Alamilla, R.; González-Chávez, M.M.; Handy, B.E.; Cárdenas-Galindo, M.G. Dehydrogenation and Diels–Alder reactions in a one-pot synthesis of benzaldehyde from n-butane over acid catalysts. *Catal. Commun.* **2012**, *27*, 154–158. [CrossRef]

11. Arce-Ramos, J.M.; Grabow, L.C.; Handy, B.E.; Cárdenas-Galindo, M.G. Nature of acid sites in silica-supported zirconium oxide: A combined experimental and periodic DFT study. *J. Phys. Chem. C* **2015**, *119*, 15150–15159. [CrossRef]

12. Vasil'ev, A.N.; Galich, P.N. Catalysts for the oxidative dehydrogenation of butenes and butane to butadiene. *Chem. Technol. Fuels Oils* **1997**, *33*, 185–192. [CrossRef]

13. Vedrine, J.C. The role of redox, acid-base and collective properties and of cristalline state of heterogeneous catalysts in the selective oxidation of hydrocarbons. *Top. Catal.* **2002**, *21*, 97–106. [CrossRef]

14. Tellez, C.; Abon, M.; Dalmon, J.A.; Mirodatos, C.; Santamaría, J. Oxidative dehydrogenation of butane over VMgO catalysts. *J. Catal.* **2000**, *195*, 113–124. [CrossRef]

15. Madeira, L.M.; Portela, M.F. Catalytic oxidative dehydrogenation of n-butane. *Catal. Rev.* **2002**, *44*, 247–286. [CrossRef]

16. Nieto, J.L.; Concepción, P.; Dejoz, A.; Knözinger, H.; Melo, F.; Vázquez, M.I. Selective oxidation of n-butane and butenes over vanadium-containing catalysts. *J. Catal.* **2000**, *189*, 147–157. [CrossRef]

17. Rostom, S.; de Lasa, H. Propane Oxidative Dehydrogenation on Vanadium-Based Catalysts under Oxygen-Free Atmospheres. *Catalysts* **2020**, *10*, 418. [CrossRef]

18. Tanimu, G.; Aitani, A.M.; Asaoka, S.; Alasiri, H. Oxidative dehydrogenation of n-butane to butadiene catalyzed by new mesoporous mixed oxides NiO-(beta-Bi_2O_3)-Bi_2SiO_5/SBA-15 system. *Mol. Catal.* **2020**, *488*, 110893. [CrossRef]

19. Wang, X.; Zhou, G.; Chen, Z.; Jiang, W.; Zhou, H. In-situ synthesis and characterization of V-MCM-41 for oxidative dehydrogenation of n-butane. *Microporous Mesoporous Mater.* **2016**, *223*, 261–267. [CrossRef]

20. Otroshchenko, T.P.; Kondratenko, V.A.; Rodemerck, U.; Linke, D.; Kondratenko, E.V. Non-oxidative dehydrogenation of propane, n-butane, and isobutane over bulk ZrO_2-based catalysts: Effect of dopant on the active site and pathways of product formation. *Catal. Sci. Technol.* **2017**, *7*, 4499–4510. [CrossRef]

21. Tanimu, G.; Abussaud, B.A.; Asaoka, S.; Alasiri, H. Kinetic Study on n-Butane Oxidative Dehydrogenation over the (Ni, Fe, Co)–Bi–O/γ-Al_2O_3 Catalyst. *Ind. Eng. Chem. Process Des. Dev.* **2020**, *59*, 2773–2780. [CrossRef]

22. Tanabe, K.; Yamaguchi, T. Acid-base bifunctional catalysis by ZrO_2 and its mixed oxides. *Catal. Today* **1994**, *20*, 185–197. [CrossRef]

23. Zhang, X.; Wang, H.; Xu, B.Q. Remarkable nanosize effect of zirconia in Au/ZrO_2 catalyst for CO oxidation. *J. Phys. Chem. B* **2005**, *109*, 9678–9683. [CrossRef]

24. Gao, X.; Wachs, I.E. Molecular engineering of supported vanadium oxide catalysts through support modification. *Top. Catal.* **2002**, *18*, 243–250. [CrossRef]

25. Li, W.; Huang, H.; Li, H.; Zhang, W.; Liu, H. Facile synthesis of pure monoclinic and tetragonal zirconia nanoparticles and their phase effects on the behavior of supported molybdena catalysts for methanol-selective oxidation. *Langmuir* **2008**, *24*, 8358–8366. [CrossRef] [PubMed]

26. Keller, D.E.; Airaksinen, S.M.; Krause, A.O.; Weckhuysen, B.M.; Koningsberger, D.C. Atomic XAFS as a tool to probe the reactivity of metal oxide catalysts: Quantifying metal oxide support effects. *J. Am. Chem. Soc.* **2007**, *129*, 3189–3197. [CrossRef]

27. Scheurell, K.; Hoppe, E.; Brzezinka, K.W.; Kemnitz, E. Bulk and surface properties of highly dispersed VOx/ZrO_2, VOx/SiO_2 and $VOx/TiO_2/SiO_2$ systems and their relevance for propane oxidation. *J. Mater. Chem.* **2004**, *14*, 2560–2568. [CrossRef]

28. Miller, J.M.; Lakshmi, L.J. Synthesis, Characterization, and Activity Studies of V_2O_5/ZrO_2–SiO_2 Catalysts. *J. Catal.* **1999**, *184*, 68–76. [CrossRef]

29. Gao, X.; Fierro, J.L.G.; Wachs, I.E. Structural characteristics and catalytic properties of highly dispersed ZrO_2/SiO_2 and $V_2O_5/ZrO_2/SiO_2$ catalysts. *Langmuir* **1999**, *15*, 3169–3178. [CrossRef]

30. Pothirat, T.; Jongsomjit, B.; Praserthdam, P. Effect of Zr-modified SiO_2-supported metallocene/MAO catalyst on copolymerization of ethylene/1-octene. *Catal. Lett.* **2008**, *121*, 266–273. [CrossRef]

31. Olthof, B.; Khodakov, A.; Bell, A.T.; Iglesia, E. Effects of support composition and pretreatment conditions on the structure of vanadia dispersed on SiO_2, Al_2O_3, TiO_2, ZrO_2, and HfO_2. *J. Phys. Chem. B* **2000**, *104*, 1516–1528. [CrossRef]

32. Rostom, S.; de Lasa, H.I. Propane Oxidative Dehydrogenation Using Consecutive Feed Injections and Fluidizable $VOx/\gamma Al_2O_3$ and VOx/ZrO_2–γAl_2O_3 Catalysts. *Ind. Eng. Chem. Res.* **2017**, *56*, 13109–13124. [CrossRef]

33. Gazzoli, D.; De Rossi, S.; Ferraris, G.; Mattei, G.; Spinicci, R.; Valigi, M. Bulk and surface structures of V_2O_5/ZrO_2 catalysts for n-butane oxidative dehydrogenation. *J. Mol. Catal. A Chem.* **2009**, *310*, 17–23. [CrossRef]

34. Gazzoli, D.; De Rossi, S.; Ferraris, G.; Valigi, M.; Ferrari, L.; Selci, S. Morphological and textural characterization of vanadium oxide supported on zirconia by ionic exchange. *Appl. Surf. Sci.* **2008**, *255*, 2012–2019. [CrossRef]

35. Su, S.C.; Bell, A.T. A study of the structure of vanadium oxide dispersed on zirconia. *J. Phys. Chem. B* **1998**, *102*, 7000–7007. [CrossRef]

36. Zou, H.; Li, M.; Shen, J.; Auroux, A. Surface acidity of supported vanadia catalysts. *J. Therm. Anal. Calorim.* **2003**, *72*, 209–221. [CrossRef]

37. Gervasini, A.; Bellussi, G.; Fenyvesi, J.; Auroux, A. Microcalorimetric and catalytic studies of the acidic character of modified metal oxide surfaces. 1. Doping ions on alumina, magnesia, and silica. *J. Phys. Chem.* **1995**, *99*, 5117–5125. [CrossRef]

38. Chary, K.V.; Ramesh, K.; Naresh, D.; Rao, P.V.R.; Rao, A.R.; Rao, V.V. The effect of zirconia polymorphs on the structure and catalytic properties of V_2O_5/ZrO_2 catalysts. *Catal. Today* **2009**, *141*, 187–194. [CrossRef]

39. Auroux, A.; Gervasini, A. Microcalorimetric study of the acidity and basicity of metal oxide surfaces. *J. Phys. Chem.* **1990**, *94*, 6371–6379. [CrossRef]

40. Roozeboom, F.; Mittelmeijer-Hazeleger, M.C.; Moulijn, J.A.; Medema, J.; De Beer, V.H.J.; Gellings, P.J. Vanadium oxide monolayer catalysts. 3. A Raman spectroscopic and temperature-programmed reduction study of monolayer and crystal-type vanadia on various supports. *J. Phys. Chem.* **1980**, *84*, 2783–2791. [CrossRef]

41. Adamski, A.; Sojka, Z.; Dyrek, K.; Che, M.; Wendt, G.; Albrecht, S. Surface heterogeneity of zirconia-supported V_2O_5 catalysts. The link between structure and catalytic properties in oxidative dehydrogenation of propane. *Langmuir* **1999**, *15*, 5733–5741. [CrossRef]

42. Chen, K.; Bell, A.T.; Iglesia, E. Kinetics and mechanism of oxidative dehydrogenation of propane on vanadium, molybdenum, and tungsten oxides. *J. Phys. Chem. B* **2000**, *104*, 1292–1299. [CrossRef]

43. Chen, B.; Munson, E.J. Investigation of the mechanism of n-butane oxidation on vanadium phosphorus oxide catalysts: Evidence from isotopic labeling studies. *J. Am. Chem. Soc.* **2002**, *124*, 1638–1652. [CrossRef] [PubMed]

44. Ballarini, N.; Cavani, F.; Cortelli, C.; Ligi, S.; Pierelli, F.; Trifiro, F.; Fumagalli, C.; Mazzoni, G.; Monti, T. VPO catalyst for n-butane oxidation to maleic anhydride: A goal achieved, or a still open challenge? *Top. Catal.* **2006**, *38*, 147–156. [CrossRef]

45. Guliants, V.V.; Carreon, M.A. Vanadium-phosphorus-oxides: From fundamentals of n-Butane oxidation to synthesis of new phases. *Catalysis* **2005**, *18*, 1–45. [CrossRef]

46. Handy, B.E.; Sharma, S.B.; Spiewak, B.E.; Dumesic, J.A. A Tian-Calvet heat-flux microcalorimeter for measurement of differential heats of adsorption. *Meas. Sci. Technol.* **1993**, *4*, 1350–1356. [CrossRef]

47. Shen, J.; Cortright, R.D.; Chen, Y.; Dumesic, J.A. Microcalorimetric and Infrared Spectroscopic Studies of γ-Al_2O_3 Modified by Basic Metal Oxides. *J. Phys. Chem.* **1994**, *98*, 8067–8073. [CrossRef]